Sodium 4-phenylbutyric acid prevents murine acetaminophen hepatotoxicity by minimizing endoplasmic reticulum stress

Hiromi Kusama, Kazuyoshi Kon, Kenichi Ikejima, Kumiko Arai,

Tomonori Aoyama, Akira Uchiyama, Shunhei Yamashina,

and Sumio Watanabe

Department of Gastroenterology, Juntendo University School of Medicine,

2-1-1 Hongo, Bunkyo-ku, Tokyo, 113-8421 Japan

Short title: PBA prevents acetaminophen liver injury

Corresponding author:

Kazuyoshi Kon, MD, PhD.

2-1-1 Hongo, Bunkyo-ku

Tokyo, 113-8421 Japan

Phone: +81-3-3813-3111, Fax: +81-3-3813-8862

E-mail: kazukon@juntendo.ac.jp

This manuscript consists of 5422 words.

Background Acetaminophen (APAP) overdose induces severe oxidative stress followed by hepatocyte apoptosis/necrosis. Previous studies have indicated that endoplasmic reticulum (ER) stress is involved in the cell death process. Therefore, we investigated the effect of the chemical chaperone 4-phenyl butyric acid (PBA) on APAP-induced liver injury in mice. ***Methods*** Eight-week-old male C57Bl6/J mice were given a single intraperitoneal (i.p.) injection of APAP (450 mg/kg body weight), following which some were repeatedly injected with PBA (120 mg/kg body weight, i.p.) every 3 h starting at 0.5 h after the APAP challenge. All mice were then serially sacrificed up to 12 h later. ***Results*** PBA treatment dramatically ameliorated the massive hepatocyte apoptosis/necrosis that was observed 6 h after APAP administration. PBA also significantly prevented the APAP-induced increases in cleaved activating transcription factor 6 and phosphorylation of c-Jun N-terminal protein kinase and significantly blunted the increases in mRNA levels for binding immunoglobulin protein, spliced X-box binding protein-1, and C/EBP homologous protein. Moreover, PBA significantly prevented APAP-induced Bax translocation to the mitochondria, and the expression of heme oxygenase-1 mRNA and 4-hydroxynonenal. By contrast, PBA did not affect hepatic glutathione depletion following APAP administration, reflecting APAP metabolism. ***Conclusions*** PBA prevents APAP-induced liver injury even when an APAP

challenge precedes its administration, suggesting its potential therapeutic utility in the clinical setting of APAP poisoning. The underlying mechanism of action most likely involves the prevention of ER stress-induced apoptosis/necrosis in the hepatocytes during APAP intoxication.

Keywords:

Endoplasmic reticulum stress; Oxidative stress; Acetaminophen; 4-phenylbutylic acid; activating transcription factor

List of abbreviations:

ALT - alanine aminotransferase

AST - aspartate aminotransferase

ANOVA - analysis of variance

eIF2α - eukaryotic initiation factor 2α

ER - endoplasmic reticulum

GAPDH - glyceraldehyde 3-phosphate dehydrogenase

GRP78 - glucose-regulated protein 78

Bip - binding immunoglobulin protein

H-E - Hematoxylin-Eosin

4-HNE - 4-hydroxy-2-nonenal

JNK- c-Jun N-terminal kinase

HO1- heme oxygenase-1

NASH - non-alcoholic steatohepatitis

sXBP1 - spliced X-box binding protein-1

UPR - unfolded protein response

NAPQI - N-Acetyl-p-Benzoquinone Imine

TUNEL - terminal deoxynucleotidyl transferase-mediated UTP end labeling

ATF6 - activating transcription factor 6

IRE1α - inositol-requiring kinase 1α

PERK - protein kinase RNA-like ER kinase

HSP60 - heat shock protein 60

GAPDH - glyceraldehyde 3-phosphate dehydrogenase

CHOP - C/EBP homologous protein

MPT - mitochondrial permeability transition

ROS - reactive oxygen species

PBA - 4-phenyl butyric acid

UPR - unfolded protein response

Conflict of interest: No potential conflicts of interest were disclosed.

Financial support:

This work was supported in part by JSPS KAKENHI (24590995 to K.K., 24590996 to K.I., 24390191 to S.W.).

Introduction

Acetaminophen (APAP) is an effective and safe analgesic/antipyretic drug that is used around the world [1]. However, the administration of excessive APAP induces severe necrosis in the hepatocytes, which rapidly progresses to acute liver failure. In the United States [2], the United Kingdom, and other countries [3-5], APAP overdose as a result of suicidal or unintentional ingestion is a critical issue [6, 7], and the incidence of APAP-induced liver injury has been increasing in Japan in recent years [8]. The first-line therapy for APAP overdose is treatment with oral N-acetyl cysteine, which is a glutathione precursor; however, this has dose-related adverse effects and limited therapeutic efficacy [9]. Therefore, it is important to explore alternative therapeutic approaches against APAP-induced hepatotoxicity.

Endoplasmic reticulum (ER) stress is a cellular stress caused by the accumulation of unfolded proteins in the ER. The response to this stress is known as the unfolded protein response (UPR) [10, 11], and involves transmembrane sensors, inositol-requiring enzyme 1 (IRE1α), protein kinase RNA-like ER kinase (PERK), and activating transcription factor 6 (ATF6). The UPR includes the induction of several molecular chaperones to restore cellular homeostasis; however, if the protein load

continues to exceed the folding capacity of the ER, cells tend to undergo apoptosis [11]. Excessive ER stress is involved in the pathogenesis of many diseases, including primary biliary cirrhosis [12], alcoholic liver injury [13], nonalcoholic fatty liver disease [14, 15], neurodegenerative diseases [16], diabetes mellitus [17, 18], viral inflammation [19], and cancer [20-22]. Some studies have also suggested that excessive ER stress contributes to APAP-induced hepatotoxicity [23, 24]. However, the usefulness of ER stress-targeting therapy on APAP-induced liver injury has not yet been established.

Chemical chaperones are small molecules that stabilize the folding of proteins and buffer abnormal protein aggregation [25]. One such molecule is sodium 4-phenylbutyric acid (PBA), which helps with the correct folding of proteins and reduces ER stress [24, 26, 27], and has been used in the treatment of urea cycle disorders [28], sickle cell disease [29], and thalassemia [30]. It has also previously been demonstrated that treatment with PBA improves murine steatohepatitis induced by fructose plus *trans*-fatty acid [31]. Therefore, in the current study, we examined the effect of PBA on APAP overdose-induced liver injury using a mouse model.

Materials and Methods

Materials

PBA and APAP were purchased from Sigma Aldrich (St. Louis, MO, USA). BIOXYTECH GSH/GSSG-412™ was purchased from OXIS Health Products, Inc. (Portland, OR, USA). Anti-4-hydroxy-2-nonenal (4-HNE) antibody was purchased from Abcam (Cambridge, MA, USA). Secondary biotinylated anti-mouse IgG, anti-c-Jun N-terminal kinase (JNK) antibody, anti-Bax antibody, anti-C/EBP homologous protein (CHOP) antibody, anti-glyceraldehyde 3-phosphate dehydrogenase (GAPDH) antibody, and anti-60-kDa member of the heat-shock protein family (HSP60) antibody were purchased from Cell Signaling Technology Inc. (Danvers, MA, USA). Anti-ATF6 antibodies was purchased from Novus Biologicals (Littleton, CO, USA) and Abcam (for cleaved ATF6 and full-length ATF6, respectively). Protease inhibitor cocktail (Complete Mini®) was purchased from Roche Diagnostics (Basel, Switzerland). All other reagents were purchased from Sigma Aldrich unless otherwise specified.

Animals and experimental design

All experimental protocols were approved by the Committee of Laboratory Animals according to the institutional guidelines. C57Bl/6J mice were purchased from CLEA Japan and housed in air-conditioned, specific pathogen-free animal quarters, with lighting from 0800 to 2000 h. The mice were given unrestricted access to a standard laboratory chow and water throughout the study.

Following acclimation, overnight-fasted 8 week-old male C57Bl/6 mice were given an intraperitoneal (i.p.) injection of APAP (450 mg/kg body weight (BW)). Some of these mice were then repeatedly injected with PBA (120 mg/kg BW, i.p.) every 3 h from 0.5–3 to 12 h after the APAP challenge. (Note: Repeated injections were given at 3-h intervals to compensate for the relatively rapid decay that PBA demonstrates *in vivo*.) The control mice were serially sacrificed up to 12 h after APAP injection, whereas the PBA-treated mice were sacrificed by blood withdrawal after 1 h, 3 h, 6 h, and 12 h. In addition, to evaluate the effect of PBA on survival following APAP administration, mice were given four repeated treatments with either PBA or serine and observed until 54 h after APAP administration.

Serum transaminase levels

The levels of serum aspartate aminotransferase (AST) and alanine aminotransferase (ALT) activity were measured colorimetrically using a Fuji DRI-CHEM system (Fuji, Japan).

Histological analysis and immunohistochemistry

For histological evaluations, liver tissues were fixed in 10% buffered formalin, embedded in paraffin, and stained with Hematoxylin and Eosin (H&E). To detect apoptotic cell death in the tissues, the terminal deoxynucleotidyl transferase-mediated dUTP nick-end labeling (TUNEL) assay was performed using a commercial kit (Deadend™ Fluorometric TUNEL system; Promega, Madison, WI, USA), according to the manufacturer's instructions. The number of TUNEL-positive nuclei was assessed using a green nuclear fluorescence dye and was divided by the total number of nuclei stained using propidium iodide (PI). Staining was quantified using laser scanning confocal microscopy (FV1000D; Olympus, Tokyo, Japan) and was performed on more than 500 hepatocytes per animal.

The expression and localization of 4-HNE in the liver tissue was detected by

immunohistochemical staining, as previously described elsewhere [32]. Briefly, deparaffinized tissue sections were incubated with a monoclonal anti-4-HNE antibody followed by secondary biotinylated anti-mouse IgG, and the specific binding was then visualized by application of the abidin–biotin complex solution followed by incubation with a 3,3-diaminobenzidine tetra hydrochloride solution using the Vectastain® Elite ABC kit (Vector Laboratories, Burlingame, CA, USA).

All of the specimens for histology and immunohistochemistry were observed under an optical microscope (Leica DM7000; Leica, Wetzlar, Germany) equipped with a digital microscope camera (MC120HD; Leica, Wetzlar, Germany).

Preparation of cytosolic and mitochondrial extract

Mitochondrial and cytosolic fractions were extracted from the livers of mice 6 h after the APAP challenge using the Mitochondria/Cytosol Fractionation Kit (Bio vision, Milpitas, CA, USA), according to the manufacturer's protocol. Briefly, after washing the livers with a physiological salt solution (PSS), they were homogenized in ice-cold cytosol extraction buffer mix containing dithiothreitol (DTT) and protease inhibitors using a Teflon homogenizer. The tissue suspensions were centrifuged at 700*g* at 4°C for

10 min, following which the supernatants were centrifuged again at 10,000*g* for 30 min to separate intact mitochondria (pellets) from the cytosolic fraction (supernatants). The pellets were then resuspended with 100 μl of mitochondrial extraction buffer mix containing DTT and protease inhibitors. The mixture was saved as the mitochondrial fraction.

Preparation of total proteins

Total protein extracts were obtained by homogenizing frozen tissues in a buffer containing 50 mM Tris (pH 8.0), 150 mM NaCl, 1 mM ethylenediaminetetraacetic acid (EDTA), 1% Triton X-100, and protease inhibitors (Complete Mini®), followed by centrifugation at 17,400*g* for 15 min. In addition, some solutions were sonicated three times for 30 s to break the Golgi membranes to allow the extraction and detection of full-length ATF6. The protein concentration was determined using a Bio-Rad protein assay kit (Bio-Rad Laboratories, Hercules, CA, USA).

Western blot analysis

Protein extracts (20 μg) were electrophoresed in 6–12% sodium dodecyl sulfate (SDS) polyacrylamide gels and electrophoretically transferred onto polyvinylidene fluoride membranes. The membranes were then blocked with 1–5% nonfat dry milk in Tris-buffered saline, and incubated with primary antibodies against JNK (anti-rabbit, 1:500), phosphorylated JNK (anti-rabbit, 1:500), cleaved ATF6 (anti-mouse monoclonal, 3:1000), full-length ATF6 (anti-rabbit, 1:100), Bax (anti-rabbit, 1:500), HSP60 (anti-rabbit, 1:500), or GAPDH (anti-rabbit, 1:500), followed by a secondary horseradish peroxidase-conjugated anti-rabbit IgG or anti-mouse IgG antibody. Specific bands were then visualized using the ECL prime detection kit (GE healthcare, Waukesha, WI, USA) and detected using an LAS3000 imaging system (Fuji Film, Japan).

RNA preparation and real-time reverse transcription polymerase chain reaction (RT-PCR)

Total RNA was prepared from frozen tissue samples using the illustra RNAspin Mini RNA Isolation kit (GE healthcare, Waukesha, WI, USA). The concentration and purity of the isolated RNA were then determined by measuring the optical density at

260 and 280 nm. For real-time RT-PCR, total RNA (1 µg) was reverse transcribed using Moloney murine leukemia virus transcriptase (SuperScript II; Invitrogen, Carlsbad, CA, USA) and an oligo (dT) 12–18 primer at 42°C for 1 h. The obtained cDNA (1 µg) was then amplified using Fast SYBR Green Master Mix® (Applied Biosystems, Foster City, CA, USA) and specific primers for CHOP (forward: AGTGCATCTTCATACACCACCACA; reverse: CAGATCCTCATACCAGGCTTCCA), heme oxygenase-1 (HO-1) (forward: CTGGAGATGACACCTGAGGTCAA; reverse: CTGACGAAGTGACGCCATCTG), GAPDH (forward: TGTGTCCGTCGTGGATCTGA; reverse: TTGCTGTTGAAGTCGCAGGAG), spliced X-box binding protein-1 (sXBP1) (forward: TGAGAACCAGGAGTTAAGAACACGC; reverse: CCTGCACCTGCTGCGGAC), and binding immunoglobulin protein (BiP) (forward: GAACACTGTGGTACCCACCAAGAA; reverse: TCCAGTCAGATCAAATGTACCCAGA). The reaction was carried out with a 10-s activation period at 95°C, followed by 40 cycles of 95°C for 5 s and 60°C for 31 s, and a final cycle of 95°C for 15 s, 60°C for 1 min, and 95°C for 15 s using the ABI PRISM® 7700 sequence detection system (PE Applied Biosystems, Foster City, CA, USA), and the threshold cycle values were obtained.

Measurement of glutathione (GSH) in the liver

Total GSH levels in the liver tissue samples were measured using a commercial kit. Briefly, livers were homogenized in cold phosphate buffered saline (PBS) supplemented with 5% mercaptopropionic acid (MPA) and the homogenate was centrifuged at 12,000 rpm for 15 min at 4°C. Liver GSH levels were then determined colorimetrically with the GSH/GSSG-412 kit and GSH contents were calculated based on the tissue protein concentration. The absorbance at 412 nm was determined using the Molecular Devices SpectraMax® 340 (Molecular Devices, Sunnyvale, CA, USA).

Statistical analysis

Data are expressed as means ± SEM. Statistical differences between the means were determined using one-way analysis of variance (ANOVA) or the Kruskal–Wallis ANOVA on ranks followed by an all pairwise multiple comparison procedure (Student–Newman–Keuls Method), as appropriate. A significance level of $P < 0.05$ was selected prior to the study.

Results

PBA protects against hepatic apoptosis/necrosis following APAP administration

Serum AST and ALT levels were significantly higher 6 h after a high-dose administration of APAP (450 mg/kg BW) than in the control (AST: 11670 ± 1670 IU/L; ALT: 11200 ± 455 IU/L). However, treatment with PBA 0.5 h after APAP administration significantly suppressed these increases ($P < 0.05$), limiting them to 2740 ± 537 IU/L for AST and 4510 ± 434 IU/L for ALT. The inhibitory effect of PBA was weakened in a time-dependent manner from the start of treatment, with the significant prevention against AST elevation being lost when the PBA treatment started 3 h after APAP administration (Fig. 1a and b)—although the increase in ALT was still significantly reduced at this time. Therefore, the PBA treatment was performed 0.5 h after APAP administration in all subsequent experiments.

Time course experiments of serum AST and ALT levels revealed that hepatic necrosis started 3 h after APAP administration (Fig. 1c and d). Serum AST and ALT levels rose rapidly until 6 h after APAP administration, following which there was a continued increase until 12 h. Similarly, PBA had a significant preventive effect on the

elevation of AST and ALT levels up to 12 h after APAP administration. To evaluate the effect of PBA on survival following an APAP overdose, mice were observed until 54 h after APAP administration following four repeated treatments with serine or PBA. All mice that received the PBA treatment survived, whereas two of the nine control mice died (Fig. 1e).

H&E staining showed that APAP induced minimal perivenular necrosis surrounded by microvesicular steatosis at 6 h, which had increased in size by 12 h after APAP administration. By contrast, PBA treatment following APAP administration dramatically attenuated the necrosis and microvesicular steatosis (Fig. 2a).

Apoptotic cell death was visualized by TUNEL staining. A large proportion of TUNEL-positive nuclei (20.6 ± 3.3% of hepatocytes) were observed predominantly in the pericentral hepatocytes at 6 h after APAP administration, which had then decreased again at 12 h after APAP administration. However, PBA treatment greatly diminished the proportion of TUNEL-positive cells at 6 h (4.0 ± 1.0%; $P < 0.05$), and this preventive effect continued through to 12 h after APAP administration (Fig. 2b and c).

Treatment with PBA reduces ER stress after exposure to APAP

To evaluate ER stress, several indicators of UPR induction were measured by western blotting, including the cleaved form of ATF6 and phosphorylated/total JNK. Cleaved ATF6 was present in both PBA-treated and untreated animals by 3 h after APAP administration. However, although the levels continued to rise by an additional 2.6 ± 0.5 fold by 6 h in the absence of PBA, they stopped rising in PBA-treated tissues (1.0 ± 0.3 fold change; $P < 0.05$, Fig. 3a and b). By contrast, there was no difference in the expression of full-length ATF6 between treatment groups over the same period. The phosphorylation of JNK also significantly increased following APAP administration, demonstrating a 37.6 ± 3.1-fold increase compared with the control. However, this increase was also significantly limited by PBA, being reduced to 26.5 ± 4.9 fold compared with the control ($P < 0.05$, Fig. 3a and c).

The expression of UPR-related mRNA was measured by real time RT-PCR. The mRNA expression of BiP and CHOP started to increase at 3 h after APAP administration, and then increased rapidly. The expression of sXBP1 mRNA was also significantly higher than the control at 6 h after APAP administration, although this increase was relatively weaker than for the other UPR-related mRNAs. However, treatment with PBA significantly blunted the mRNA expression of BiP, sXBP1, and CHOP ($P < 0.05$, Fig. 3d–f, $P < 0.05$).

PBA prevents APAP-induced Bax translocation to the mitochondria

Western blotting using cytosolic and mitochondrial fractions from the liver at 6 h after APAP administration showed that Bax had significantly increased in the mitochondrial fraction, climbing to 6.0 ± 1.9 fold higher than the control value ($P < 0.05$). However, treatment with PBA significantly suppressed this increase, limiting the increase in Bax levels in the mitochondrial fraction to 2.9 ± 0.9 fold higher than the control ($P < 0.05$, Fig. 4a and b). By contrast, Bax levels in the cytosolic fraction tended to decrease following APAP administration, although this difference was not statistically significant (Fig. 4a and c).

PBA prevents an APAP-induced increase in oxidative stress

Immunohistological staining of 4-HNE showed that APAP administration led to the consistently localized enhancement of oxidative stress with necrosis of the hepatocytes, which was prevented by PBA (Fig. 5a). Furthermore, APAP significantly increased the levels of HO-1 mRNA, leading to a 97.3 ± 1.6-fold increase in the liver at 6 h after the

APAP challenge, and PBA also significantly suppressed this, limiting it to a 49.3 ± 8.4-fold increase ($P < 0.05$, Fig. 5b). To evaluate the effect of PBA on APAP metabolism, GSH depletion was measured through the early phase up to 3 h after APAP administration. There was a rapid depletion of GSH content in the liver at 1–3 h after APAP administration. However, PBA did not affect this depletion after 1 h or the recovery after 3 h (Fig. 5c).

Discussion

In the present study, a large APAP overdose caused microvesicular steatosis, massive hepatocyte apoptosis/necrosis predominantly in the central areas~~, and~~ and markedly enhanced levels of serum transaminase. It has previously been reported that ER stress causes microvesicular hepatic steatosis [33], and so fat accumulation may enhance the increased ER stress in the hepatocytes. The number of apoptotic cells had decreased by 12 h after APAP administration (Fig. 2b), possibly indicating that the apoptotic cells underwent secondary necrosis at this stage. Repeated treatment with PBA diminished microvesicular steatosis, and strongly suppressed both the necrosis and apoptosis caused by~~after~~ APAP (Figs. 1 and 2).

To evaluate the effect of PBA on ER stress in APAP-induced liver injury, we measured the expression of UPR-related mRNA and proteins in the liver. We found that PBA markedly suppressed the activation of ATF6 and JNK, as well as subsequent expression of CHOP during APAP-induced hepatotoxicity (Fig. 3). UPR signaling attenuates protein synthesis to prevent further protein aggregation and accumulation in the ER, but if this ultimately fails, cell death ensues [10, 34, 35]. It has previously been

suggested that ATF6 cleavage plays a critical role in the development of APAP-induced liver injury via activation of the pro-apoptotic protein CHOP [11, 23, 24]. Full-length ATF6 is localized at the ER membrane and bound to the ER-localized chaperone BiP, which is released in response to ER stress. This BiP dissociation induces ATF6 translocation to the Golgi apparatus, where it is cleaved by proteases [9-11] leading to the induction of several transcription factors, including CHOP [36-38] and XBP1 [39]. It has already been reported that the cleavage of ATF6 in the ER stress-CHOP pathway plays a crucial role in APAP hepatotoxicity [23, 24], and that JNK activation also plays a major role [40, 41]. Furthermore, the phosphorylation of JNK increases the expression of CHOP in animal models [42, 43]. Thus, it is concluded that the PBA treatment minimized ER stress after APAP administration by suppressing both the ATF6-CHOP and JNK-CHOP pathways.

Our data indicated that APAP-induced Bax translocation to the mitochondrial fraction, and that this translocation was significantly inhibited by PBA (Fig. 4). Furthermore, immunohistological staining for 4HNE, a major biomarker of oxidative stress and lipid peroxidation, revealed that treatment with PBA markedly improved the oxidative stress that was observed predominantly in the pericentral area after APAP

administration; and real-time RT-PCR for HO-1 mRNA, an oxidative stress-inducible protein localized in the mitochondria, demonstrated that mitochondrial oxidative stress after APAP administration was strongly suppressed by PBA (Fig. 5a and b). Excessive accumulation of reactive oxygen species (ROS) results in several types of hepatocyte injury, including protein oxidation, lipid peroxidation, and DNA damage. Mitochondria are a major source of ROS generation and play a critical role in APAP-induced hepatotoxicity [44], with the translocation of Bax from the cytosol to the mitochondria being a critical step in the mitochondrial death pathway [45, 46]. It has previously been shown that excessive APAP induces iron-dependent mitochondrial oxidative stress followed by mitochondrial permeability transition (MPT), which leads to ATP-synthesis-dependent hepatic necrosis and apoptosis [8, 9, 47, 48]. Therefore, we reasoned that PBA treatment following APAP administration prevented the crucial death pathway in hepatocytes by ameliorating mitochondrial oxidative stress following the translocation of Bax to the mitochondria.

Previous studies have indicated that the interaction between the ER and mitochondria plays an important role in ER stress- and oxidative stress-related cell injury. The ER forms close contacts with the mitochondria via a domain known as the

mitochondria-associated membrane [49]. The release of calcium ions, membrane proteins, UPR-related signal proteins, and unfolded protein-induced ROS from the ER to the mitochondria leads to impaired mitochondrial respiration and increased mitochondrial ROS [34, 50-52]. Our findings suggest that PBA prevented the trafficking of these molecules to the mitochondria by reducing APAP-induced ER stress. The preventive effect of PBA on the expression of CHOP, sXBP1, and BiP mRNA was lost at 12 h after APAP administration; however, oxidative stress was still blunted by PBA at this time, and mice that were treated with PBA were still alive at 52 h after APAP administration. This may indicate that CHOP requires some other UPR-related signal activation to induce the lethal death pathway.

PBA did not affect the APAP-induced early reduction in hepatic GSH levels 1 h after APAP administration (Fig. 5c). At therapeutic doses, APAP is primarily eliminated as its glucuronide and sulfate conjugate; however, following an overdose, APAP is oxidized to N-acetyl-p-benzoquinone imine (NAPQI) [6], which is a reactive metabolite. NAPQI is detoxified by conjugation with GSH, causing GSH depletion [53], and also immediately conjugates with proteins, resulting in APAP-protein adduct formation followed by cell toxicity [54]. Thus, the production of NAPQI can be indirectly

evaluated by assessing the level of GSH depletion after APAP administration [53]. Treatment with N-acetyl cysteine prevents GSH depletion after an APAP overdose [55]. Therefore, the finding that PBA treatment does not affect the reduction in GSH indicates that the protective effect of PBA on APAP-hepatotoxicity is unrelated to any changes in APAP metabolism, and that the therapeutic target of PBA is located further downstream than N-acetyl cysteine.

In this study, PBA was repeatedly administered at 3-h intervals because it has been shown to decay relatively rapidly *in vivo* [56]. We also tested the effect of PBA following a single injection 0.5 h after APAP administration; however, the protective effect was weaker than with a repeated injection at 6 h, with protection being lost by 12 h after APAP administration (data not shown). A previous study showed that pre- and post-treatment with a single dose of PBA prevented serum transaminase elevation after APAP administration, and that pretreatment with PBA prevented hepatic XBP1 mRNA splicing and JNK phosphorylation; however, the effect against the ER stress markers in the liver was lost when mice received a post-treatment with PBA [57]. Since many cases of APAP-induced liver injury occur as a result of suicidal intent [2], the effectiveness of post-exposure treatment has greater clinical relevance.

Conclusions

Our findings indicate that an APAP overdose causes hepatic apoptosis/necrosis through an increase in ER stress and oxidative stress. The cleavage of ATF6, phosphorylation of JNK, and increase in mitochondrial oxidative stress are critical components of this toxicity. Treatment with PBA dramatically reduced hepatic apoptosis/necrosis after APAP administration by preventing both ER stress and subsequent mitochondrial oxidative stress. Therefore, treatment with PBA targeting ER stress is a promising novel approach for preventing or minimizing APAP-induced liver injury.

Acknowledgments

The authors thank Takako Ikegami and Tomomi Ikeda (Laboratory of Molecular and Biochemical Research, Research Support Center, Juntendo University Graduate School of Medicine, Tokyo, Japan) and Maiko Suzuki and Ryota Kitagawa (Department of Gastroenterology, Juntendo University School of Medicine, Tokyo, Japan) for technical assistance and R. F. Whittier for critical reading of the manuscript and thoughtful discussions.

References

1. Brune K, Renner B, Tiegs G. Acetaminophen/paracetamol: A history of errors, failures and false decisions. Eur J Pain 2015;19:953-65.

2. Major JM, Zhou EH, Wong HL, et al. Trends in rates of acetaminophen-related adverse events in the United States. Pharmacoepidemiol Drug Saf 2016;25(5):590-8.

3. Canbay A, Jochum C, Bechmann LP, et al. Acute liver failure in a metropolitan area in Germany: a retrospective study (2002 - 2008). Z Gastroenterol 2009;47:807-13.

4. Krenzelok EP. The FDA Acetaminophen Advisory Committee Meeting - what is the future of acetaminophen in the United States? The perspective of a committee member. Clin Toxicol (Phila) 2009;47:784-9.

5. Xu C, Bailly-Maitre B, Reed JC. Endoplasmic reticulum stress: cell life and death decisions. J Clin Invest 2005;115:2656-64.

6. Ferner RE, Dear JW, Bateman DN. Management of paracetamol poisoning. BMJ 2011;342:d2218.

7. Zyoud SH, Al-Jabi SW, Sweileh WM, et al. Global research productivity of N-acetylcysteine use in paracetamol overdose: A bibliometric analysis (1976-2012). Hum Exp Toxicol 2015;34:1006-16.

8. Sudo C, Maekawa K, Segawa K, et al. [Trends in drug-induced liver injury

based on reports of adverse reactions to PMDA in Japan]. Kokuritsu Iyakuhin Shokuhin Eisei Kenkyusho Hokoku 2012:66-70.

9. Chiew AL, Isbister GK, Duffull SB, et al. Evidence for the changing regimens of acetylcysteine. Br J Clin Pharmacol 2016;81:471-81.

10. Doyle KM, Kennedy D, Gorman AM, et al. Unfolded proteins and endoplasmic reticulum stress in neurodegenerative disorders. J Cell Mol Med 2011;15:2025-39.

11. Sano R, Reed JC. ER stress-induced cell death mechanisms. Biochim Biophys Acta 2013;1833:3460-70.

12. Sasaki M, Yoshimura-Miyakoshi M, Sato Y, et al. A possible involvement of endoplasmic reticulum stress in biliary epithelial autophagy and senescence in primary biliary cirrhosis. J Gastroenterol 2015;50:984-95.

13. Du RH, Tan J, Yan N, et al. Kir6.2 knockout aggravates lipopolysaccharide-induced mouse liver injury via enhancing NLRP3 inflammasome activation. J Gastroenterol 2014;49:727-36.

14. Hamano M, Ezaki H, Kiso S, et al. Lipid overloading during liver regeneration causes delayed hepatocyte DNA replication by increasing ER stress in mice with simple hepatic steatosis. J Gastroenterol 2014;49:305-16.

15. Narabayashi K, Ito Y, Eid N, et al. Indomethacin suppresses LAMP-2

expression and induces lipophagy and lipoapoptosis in rat enterocytes via the ER stress pathway. J Gastroenterol 2015;50:541-54.

16. Prentice H, Modi JP, Wu JY. Mechanisms of Neuronal Protection against Excitotoxicity, Endoplasmic Reticulum Stress, and Mitochondrial Dysfunction in Stroke and Neurodegenerative Diseases. Oxid Med Cell Longev 2015;2015:964518.

17. Salvado L, Palomer X, Barroso E, et al. Targeting endoplasmic reticulum stress in insulin resistance. Trends Endocrinol Metab 2015;26:438-48.

18. Zhang Q, Li Y, Liang T, et al. ER stress and autophagy dysfunction contribute to fatty liver in diabetic mice. Int J Biol Sci 2015;11:559-68.

19. Hrincius ER, Liedmann S, Finkelstein D, et al. Acute Lung Injury Results from Innate Sensing of Viruses by an ER Stress Pathway. Cell Rep 2015;11:1591-603.

20. Asano T, Sato A, Isono M, et al. Bortezomib and belinostat inhibit renal cancer growth synergistically by causing ubiquitinated protein accumulation and endoplasmic reticulum stress. Biomed Rep 2015;3:797-801.

21. He J, Du L, Bao M, et al. Oroxin A inhibits breast cancer cell growth by inducing robust endoplasmic reticulum stress and senescence. Anticancer Drugs 2016;27:204-15.

22. Zhang T, Kho DH, Wang Y, et al. Gp78, an E3 ubiquitin ligase acts as a

gatekeeper suppressing nonalcoholic steatohepatitis (NASH) and liver cancer. PLoS One 2015;10:e0118448.

23. Uzi D, Barda L, Scaiewicz V, et al. CHOP is a critical regulator of acetaminophen-induced hepatotoxicity. J Hepatol 2013;59:495-503.

24. Nagy G, Kardon T, Wunderlich L, et al. Acetaminophen induces ER dependent signaling in mouse liver. Arch Biochem Biophys 2007;459:273-9.

25. Song YF, Luo Z, Zhang LH, et al. Endoplasmic reticulum stress and disturbed calcium homeostasis are involved in copper-induced alteration in hepatic lipid metabolism in yellow catfish Pelteobagrus fulvidraco. Chemosphere 2015;144:2443-53.

26. Kolb PS, Ayaub EA, Zhou W, et al. The therapeutic effects of 4-phenylbutyric acid in maintaining proteostasis. Int J Biochem Cell Biol 2015;61:45-52.

27. Vilatoba M, Eckstein C, Bilbao G, et al. Sodium 4-phenylbutyrate protects against liver ischemia reperfusion injury by inhibition of endoplasmic reticulum-stress mediated apoptosis. Surgery 2005;138:342-51.

28. Lichter-Konecki U, Diaz GA, Merritt JL, 2nd, et al. Ammonia control in children with urea cycle disorders (UCDs); phase 2 comparison of sodium phenylbutyrate and glycerol phenylbutyrate. Mol Genet Metab 2011;103:323-9.

29. Odievre MH, Brun M, Krishnamoorthy R, et al. Sodium phenyl butyrate

downregulates endothelin-1 expression in cultured human endothelial cells: relevance to sickle-cell disease. Am J Hematol 2007;82:357-62.

30. Collins AF, Pearson HA, Giardina P, et al. Oral sodium phenylbutyrate therapy in homozygous beta thalassemia: a clinical trial. Blood 1995;85:43-9.

31. Morinaga M, Kon K, Saito H, et al. Sodium 4-phenylbutyrate prevents murine dietary steatohepatitis caused by trans-fatty acid plus fructose. J Clin Biochem Nutr 2015;57:183-91.

32. Kon K, Ikejima K, Okumura K, et al. Diabetic KK-A(y) mice are highly susceptible to oxidative hepatocellular damage induced by acetaminophen. Am J Physiol Gastrointest Liver Physiol 2010;299:G329-37.

33. Jo H, Choe SS, Shin KC, et al. Endoplasmic reticulum stress induces hepatic steatosis via increased expression of the hepatic very low-density lipoprotein receptor. Hepatology 2013;57:1366-77.

34. Harding HP, Zhang Y, Ron D. Protein translation and folding are coupled by an endoplasmic-reticulum-resident kinase. Nature 1999;397:271-4.

35. Ma Y, Hendershot LM. Delineation of a negative feedback regulatory loop that controls protein translation during endoplasmic reticulum stress. J Biol Chem 2003;278:34864-73.

36. Shen J, Chen X, Hendershot L, et al. ER stress regulation of ATF6 localization by dissociation of BiP/GRP78 binding and unmasking of Golgi localization signals. Dev Cell 2002;3:99-111.

37. Yoshida H, Okada T, Haze K, et al. ATF6 activated by proteolysis binds in the presence of NF-Y (CBF) directly to the cis-acting element responsible for the mammalian unfolded protein response. Mol Cell Biol 2000;20:6755-67.

38. Fu HY, Minamino T, Tsukamoto O, et al. Overexpression of endoplasmic reticulum-resident chaperone attenuates cardiomyocyte death induced by proteasome inhibition. Cardiovasc Res 2008;79:600-10.

39. Yoshida H, Matsui T, Yamamoto A, et al. XBP1 mRNA is induced by ATF6 and spliced by IRE1 in response to ER stress to produce a highly active transcription factor. Cell 2001;107:881-91.

40. Du K, Xie Y, McGill MR, et al. Pathophysiological significance of c-jun N-terminal kinase in acetaminophen hepatotoxicity. Expert Opin Drug Metab Toxicol 2015;11:1769-79.

41. Saito C, Lemasters JJ, Jaeschke H. c-Jun N-terminal kinase modulates oxidant stress and peroxynitrite formation independent of inducible nitric oxide synthase in acetaminophen hepatotoxicity. Toxicol Appl Pharmacol 2010;246:8-17.

42. McCullough KD, Martindale JL, Klotz LO, et al. Gadd153 sensitizes cells to endoplasmic reticulum stress by down-regulating Bcl2 and perturbing the cellular redox state. Mol Cell Biol 2001;21:1249-59.

43. Puthalakath H, O'Reilly LA, Gunn P, et al. ER stress triggers apoptosis by activating BH3-only protein Bim. Cell 2007;129:1337-49.

44. Lee CH, Kuo CY, Wang CJ, et al. A polyphenol extract of Hibiscus sabdariffa L. ameliorates acetaminophen-induced hepatic steatosis by attenuating the mitochondrial dysfunction in vivo and in vitro. Biosci Biotechnol Biochem 2012;76:646-51.

45. Bulku E, Stohs SJ, Cicero L, et al. Curcumin exposure modulates multiple pro-apoptotic and anti-apoptotic signaling pathways to antagonize acetaminophen-induced toxicity. Curr Neurovasc Res 2012;9:58-71.

46. Xu C, Xu W, Palmer AE, et al. BI-1 regulates endoplasmic reticulum Ca2+ homeostasis downstream of Bcl-2 family proteins. J Biol Chem 2008;283:11477-84.

47. Kon K, Kim JS, Uchiyama A, et al. Lysosomal iron mobilization and induction of the mitochondrial permeability transition in acetaminophen-induced toxicity to mouse hepatocytes. Toxicol Sci 2010;117:101-8.

48. Uchiyama A, Kim JS, Kon K, et al. Translocation of iron from lysosomes into mitochondria is a key event during oxidative stress-induced hepatocellular injury.

Hepatology 2008;48:1644-54.

49. Simmen T, Lynes EM, Gesson K, et al. Oxidative protein folding in the endoplasmic reticulum: tight links to the mitochondria-associated membrane (MAM). Biochim Biophys Acta 2010;1798:1465-73.

50. Salem IB, Prola A, Boussabbeh M, et al. Activation of ER stress and apoptosis by alpha- and beta -Zearalenol in HCT116 cells, protective role of Quercetin. Neurotoxicology 2016;53:334-42.

51. Zhong D, Wang H, Liu M, et al. Ganoderma lucidum polysaccharide peptide prevents renal ischemia reperfusion injury via counteracting oxidative stress. Sci Rep 2015;5:16910.

52. Egnatchik RA, Leamy AK, Jacobson DA, et al. ER calcium release promotes mitochondrial dysfunction and hepatic cell lipotoxicity in response to palmitate overload. Mol Metab 2014;3:544-53.

53. Xie Y, McGill MR, Dorko K, et al. Mechanisms of acetaminophen-induced cell death in primary human hepatocytes. Toxicol Appl Pharmacol 2014;279:266-74.

54. Larson AM. Acetaminophen hepatotoxicity. Clin Liver Dis 2007;11:525-48, vi.

55. Lauterburg BH, Corcoran GB, Mitchell JR. Mechanism of action of N-acetylcysteine in the protection against the hepatotoxicity of acetaminophen in rats in

vivo. J Clin Invest 1983;71:980-91.

56. Gilbert J, Baker SD, Bowling MK, et al. A phase I dose escalation and bioavailability study of oral sodium phenylbutyrate in patients with refractory solid tumor malignancies. Clin Cancer Res 2001;7:2292-300.

57. Shimizu D, Ishitsuka Y, Miyata K, et al. Protection afforded by pre- or post-treatment with 4-phenylbutyrate against liver injury induced by acetaminophen overdose in mice. Pharmacol Res 2014;87:26-41.

Figure Legends

Fig. 1.

Post-treatment with 4-phenylbutyric acid (PBA) prevents the elevation of serum transaminase levels and keeps mice alive following an acetaminophen (APAP) overdose. **a, b** Serum aspartate aminotransferase (AST; **a)** and alanine aminotransferase (ALT; **b)** levels were measured at 6 h after intraperitoneal APAP administration (450 mg/kg body weight (BW)) in mice treated with PBA at start times ranging from 0.5 to 3 h after APAP administration. **c, d** Time course of serum AST (**c)** and ALT (**d**) levels in mice treated with PBA 0.5 h after APAP administration (n = 5; * $P < 0.05$ vs. control; # $P < 0.05$ vs. APAP; ANOVA on ranks and Student–Neuman–Keuls post-hoc test). **e** Kaplan–Meier survival plot of mice treated with PBA or serine 0.5 h after APAP administration (n = 9).

Fig. 2.

The effect of 4-phenylbutyric acid (PBA) on acetaminophen (APAP)-induced hepatic apoptosis/necrosis. C57Bl/6 mice were given an intraperitoneal (i.p.) injection of APAP (450 mg/kg body weight (BW)). Some of these mice were then treated with PBA (120 mg/kg BW, i.p.) at 30 min after APAP administration. **a** Representative photomicrographs of H&E staining of the liver at 3, 6, and 12 h after APAP administration; original magnification: 100×, scale bar: 100 μm. **b** Representative photomicrographs of TUNEL staining of the liver at 3, 6, and 12 h after APAP administration; original magnification, 100×; scale bar, 100 μm. **c** TUNEL-positive cells were counted and expressed as a percentage of the total cells at 6 h after APAP administration (n = 5; * $P < 0.05$ vs. control; # $P < 0.05$ vs. APAP; ANOVA on ranks and Student–Neuman–Keuls post-hoc test).

Fig. 3.

The effect of 4-phenylbutyric acid (PBA) on acetaminophen (APAP)-induced endoplasmic reticulum stress in the liver tissue. C57Bl/6 mice were given an intraperitoneal (i.p.) injection of APAP (450 mg/kg body weight (BW)), following which some mice were treated with PBA (120 mg/kg BW, i.p.) at 30 min after APAP administration. Livers were obtained from the mice up to 12 h after APAP administration. The expression of full-length and cleaved activating transcription factor 6 (f-ATF6 and c-ATF6, respectively), phosphorylated/total-c-Jun N-terminal protein kinase (JNK), and glyceraldehyde 3-phosphate dehydrogenase (GAPDH) were detected by western blotting. **a** Representative blots. **b, c** Densitometric quantification of each protein from the immunoblots. Cleaved ATF6 and phosphorylated JNK were normalized to GAPDH and total JNK, respectively, and data were compared with the control. **d–f** Binding immunoglobulin protein (BiP), spliced X-box binding protein-1 (XBP1), and C/EBP homologous protein (CHOP) mRNA levels in the liver were measured at up to 12 h after the APAP challenge by real-time reverse transcription polymerase chain reaction (RT-PCR). (n = 5; * $P < 0.05$ vs. control; # $P < 0.05$ vs. APAP; ANOVA on ranks and Student–Neuman–Keuls post-hoc test.)

Fig. 4.

The effect of 4-phenyl butyric acid (PBA) on acetaminophen (APAP)-induced Bax translocation. C57Bl/6 mice were given an intraperitoneal (i.p.) injection of APAP (450 mg/kg body weight (BW)), and 30 min later, some of these mice were treated with PBA (120 mg/kg BW, i.p.). Livers were obtained from the mice, and the mitochondrial and cytosol fractions were separated out at 6 h after APAP administration. The presence of Bax in the mitochondria (m-Bax) or cytosol (c-Bax), as well as the expression of the 60-kDa member of the heat-shock protein family (HSP60) and glyceraldehyde 3-phosphate dehydrogenase (GAPDH) was detected by western blotting. **a** Representative blots. **b** The expression of Bax normalized by HSP60 in the mitochondrial fractions. **c** The expression of Bax normalized by GAPDH in the cytosol. (n = 5; * $P < 0.05$ vs. control; # $P < 0.05$ vs. APAP; ANOVA on ranks and Student–Neuman–Keuls post-hoc test.)

Fig. 5.

The effect of 4-phenyl butyric acid (PBA) on oxidative stress and glutathione (GSH) depletion following an acetaminophen (APAP) overdose. C57Bl/6 mice were given an intraperitoneal (i.p.) injection of APAP (450 mg/kg body weight (BW)), and 30 min later, some of these mice were treated with PBA (120 mg/kg BW, i.p.). Livers were obtained from the mice at 3–12 h after APAP administration. **a** Representative photographs of immunohistochemical staining of the livers for 4-hydroxy-2-nonenal (4-HNE) at 12 h after APAP administration; original magnification, 100×; scale bar, 100 μm. **b** The expression of heme oxygenase-1 (HO-1) mRNA in the livers at up to 12 h after APAP administration measured by real-time reverse transcription polymerase chain reaction (RT-PCR). **c** Total protein-normalized GSH levels at 1 or 3 h after APAP administration. (n = 5; * $P < 0.05$ vs. control; # $P < 0.05$ vs. APAP; ANOVA on ranks and Student–Neuman–Keuls post-hoc test.)

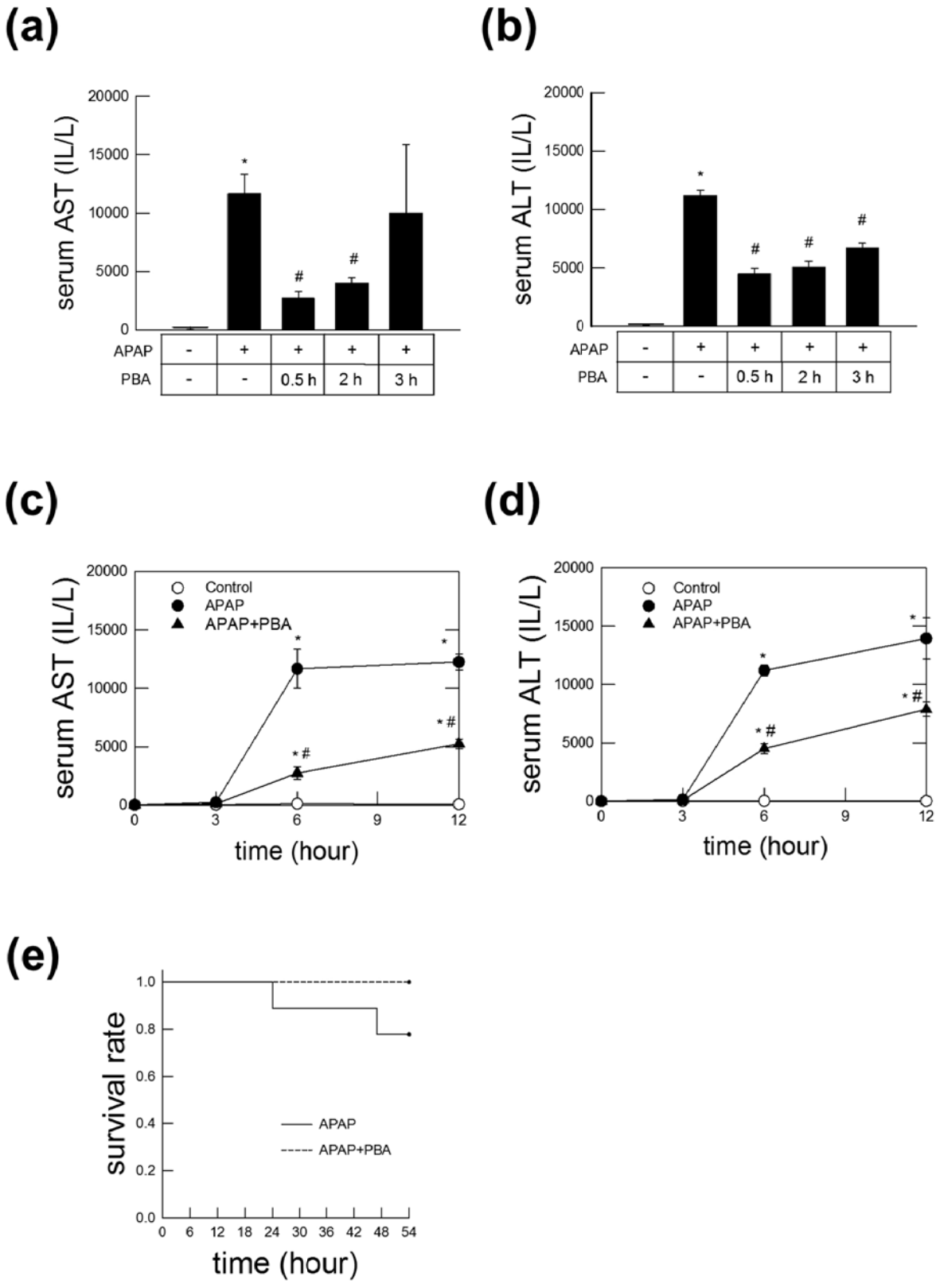
(a)
serum AST (IL/L)
20000
15000
10000
5000
0
APAP - + + + +
PBA - - 0.5 h 2 h 3 h
(b)
serum ALT (IL/L)
20000
15000
10000
5000
0
APAP - + + + +
PBA - - 0.5 h 2 h 3 h
(c)
serum AST (IL/L)
Control
APAP
APAP+PBA
time (hour)
0 3 6 9 12
(d)
serum ALT (IL/L)
Control
APAP
APAP+PBA
time (hour)
0 3 6 9 12
(e)
survival rate
1.0
0.8
0.6
0.4
0.2
0.0
APAP
APAP+PBA
0 6 12 18 24 30 36 42 48 54
time (hour)

Fig. 1

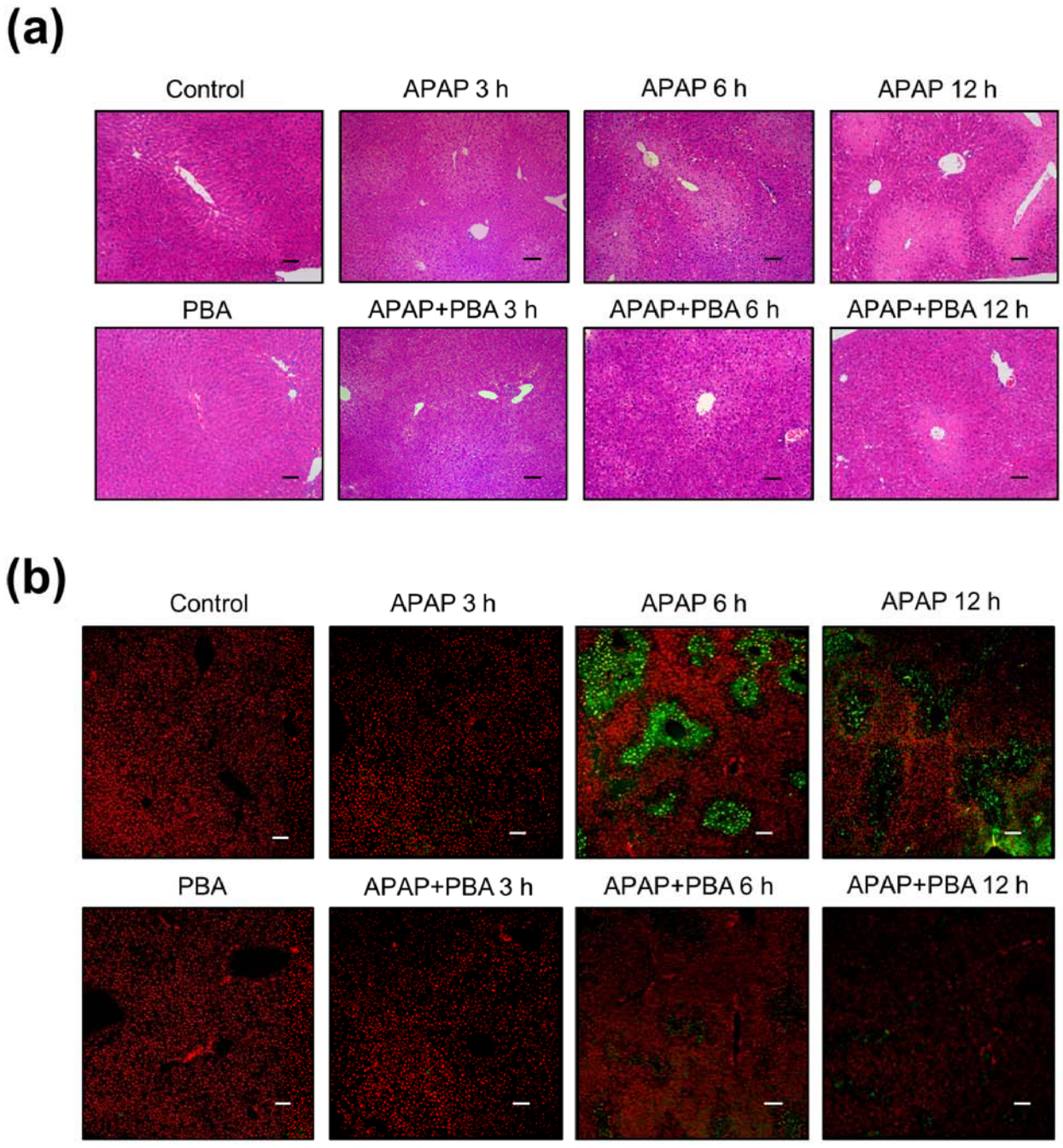
(a)
Control
APAP 3 h
APAP 6 h
APAP 12 h
PBA
APAP+PBA 3 h
APAP+PBA 6 h
APAP+PBA 12 h
(b)
Control
APAP 3 h
APAP 6 h
APAP 12 h
PBA
APAP+PBA 3 h
APAP+PBA 6 h
APAP+PBA 12 h
(c)
TUNEL positive (%)
25
20
15
10
5
0
*
*#
Control
PBA
AAP
AAP+PBA

Fig. 2

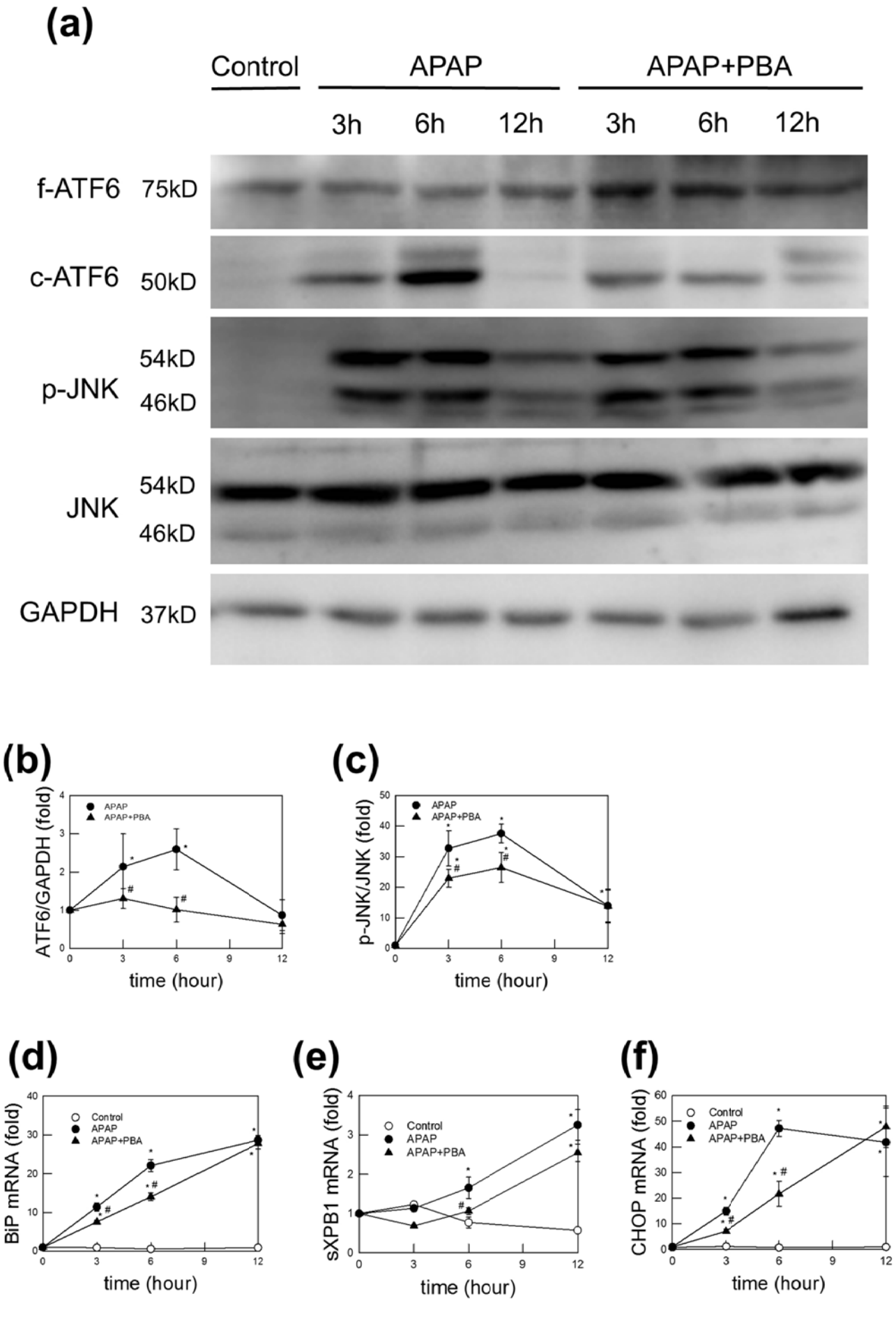
(a)
Control
APAP
APAP+PBA
3h
6h
12h
3h
6h
12h
f-ATF6 75kD
c-ATF6 50kD
p-JNK 54kD 46kD
JNK 54kD 46kD
GAPDH 37kD
(b)
ATF6/GAPDH (fold)
APAP
APAP+PBA
time (hour)
(c)
p-JNK/JNK (fold)
APAP
APAP+PBA
time (hour)
(d)
BiP mRNA (fold)
Control
APAP
APAP+PBA
time (hour)
(e)
sXPB1 mRNA (fold)
Control
APAP
APAP+PBA
time (hour)
(f)
CHOP mRNA (fold)
Control
APAP
APAP+PBA
time (hour)

Fig. 3

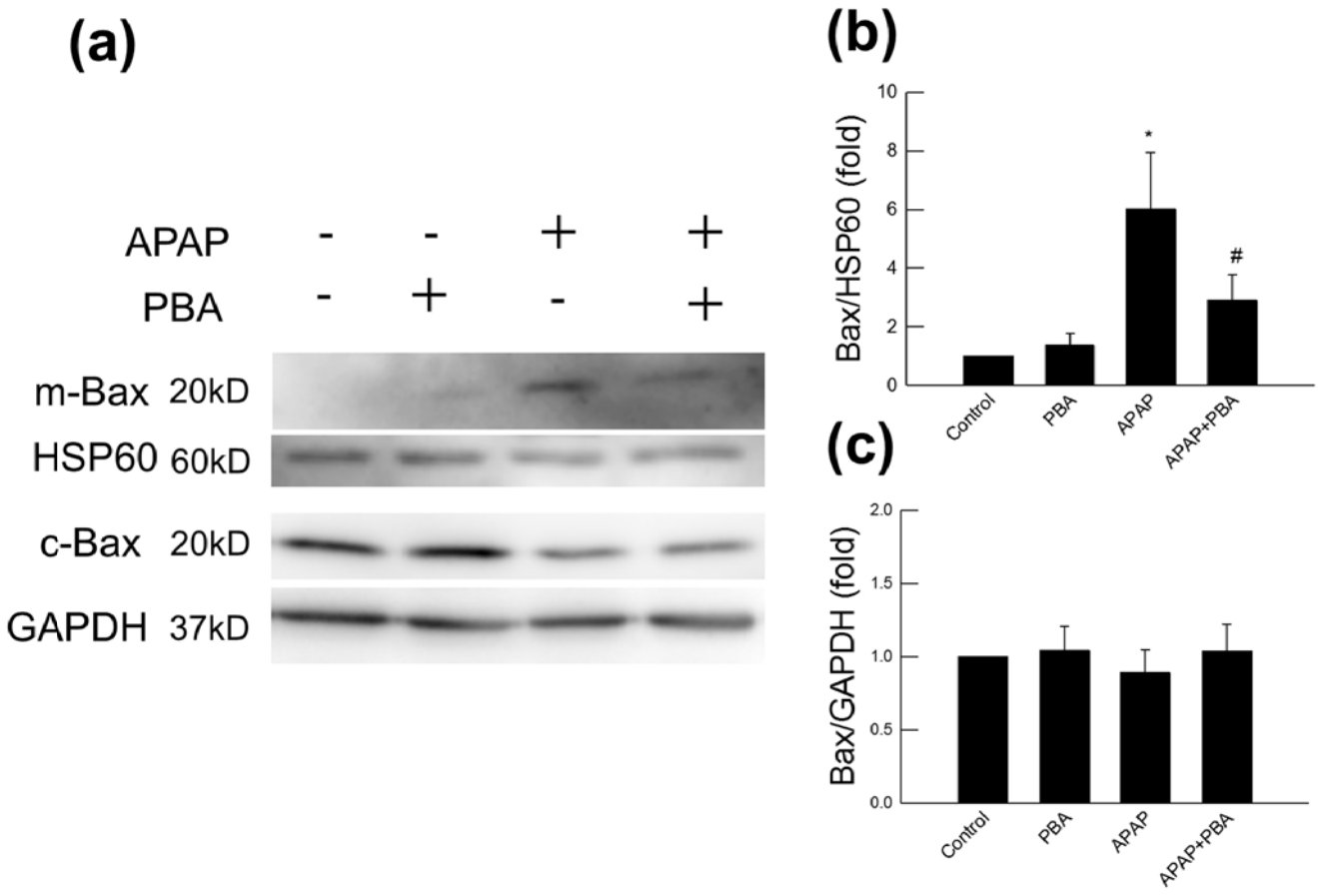
(a)
APAP - - + +
PBA - + - +
m-Bax 20kD
HSP60 60kD
c-Bax 20kD
GAPDH 37kD
(b)
Bax/HSP60 (fold)
10
8
6
4
2
0
*
#
Control
PBA
APAP
APAP+PBA
(c)
Bax/GAPDH (fold)
2.0
1.5
1.0
0.5
0.0
Control
PBA
APAP
APAP+PBA

Fig. 4

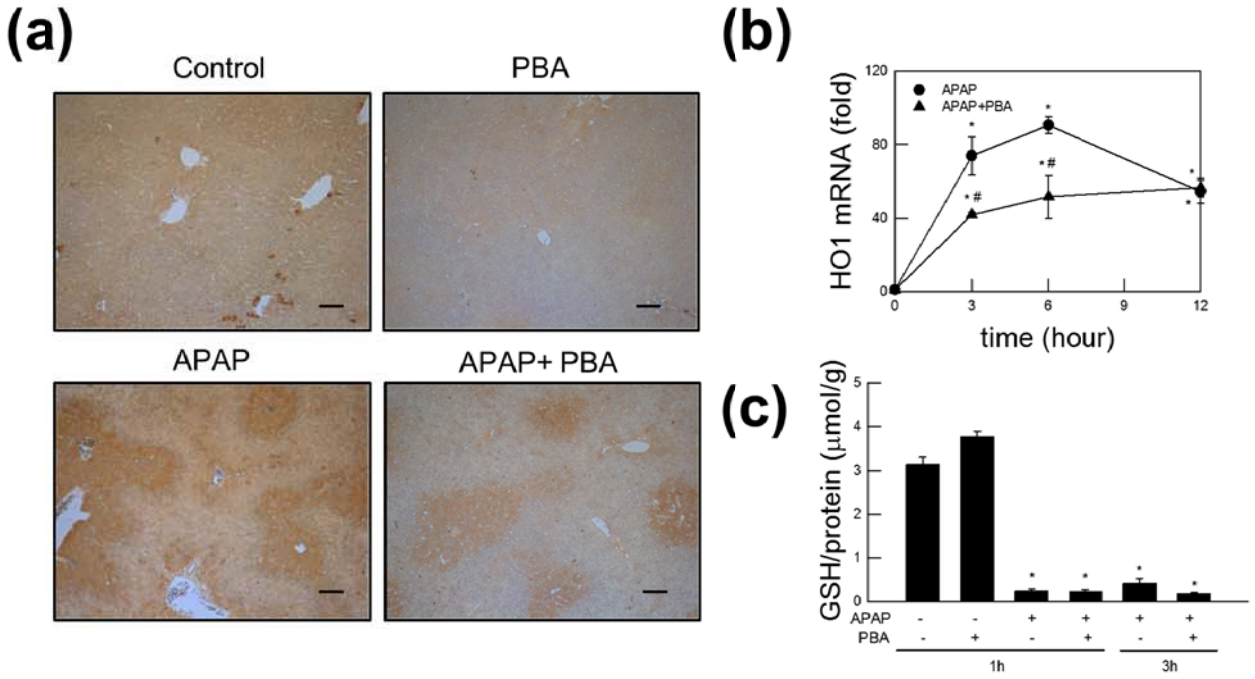
(a)
Control
PBA
APAP
APAP+ PBA
(b)
APAP
APAP+PBA
HO1 mRNA (fold)
120
80
40
0
0
3
6
9
12
time (hour)
(c)
GSH/protein (μmol/g)
5
4
3
2
1
0
APAP
PBA
1h
3h

Fig. 5